

## 2. Methods

### 2.1. Overview

For this project we used different methods, which are shortly introduced in this chapter: analyses of structural data, estimation of PT conditions, image analyses for clast scaling, structural restoration of cross section, provenance analyses, analyses of Sr isotope signatures, and Rb/Sr as well as Ar/Ar geochronology. The results of the different methods can be found within the subsequent chapters. In addition, the sample preparation procedures for Rb/Sr, Ar/Ar and Sr isotope analyses are also mentioned within Chapters 4, 5 and 6, because they are part of submitted publications. Microscopic investigations are not mentioned explicitly, because they are the basics for most of the above mentioned methods.

### 2.2. Analyses of structural data

Structural data were collected during field campaigns in summer 2004, 2005 and 2006 in the Western Alps (Eastern Switzerland and Western Austria). Foliation, lineation, shear bands, fold axes, mineralized veins and pseudotachylytes were measured, their distribution and density, geometric proportions, as well as relative age relationships were determined in the field. We investigated shear sense indicators like drag folds and the orientation of shear bands to assess the direction of tectonic transport for the hanging wall.

### 2.3. PT estimates

Geothermobarometry is used to calculate metamorphic temperature and pressure conditions. Therefore, the metamorphic paragenesis has to be in a chemical

equilibrium in order to fulfill the following equation:

$$\Delta G = 0 \quad [1]$$

where G is the Gibbs free energy. If the change of the Gibbs free energy equals 0, no reaction occurs and the system is in an equilibrium state.

Most geothermobarometers are based on element exchange during mineral reactions (univariate, continuously or cation exchange), but there are also other methods based on e.g. net transfer reactions or solvus thermometry. It is not the aim of this study to explain the different geothermobarometers, but the interested reader is referred to Spear (1995) for overview information. The use of different methods for PT estimates was constrained by the limited paragenesis associated with Alpine deformation and metamorphism in the study area (diagenetic to lowest greenschist facies conditions in the northern part, roughly upper greenschist facies conditions towards the south), because geothermobarometry is more difficult with paragenesis formed at low PT conditions.

The thermodynamic basics for geothermobarometry are expressed in equation [2],

$$\left( \frac{\partial P}{\partial T} \right)_{\ln(K_{eq})} = \frac{\Delta S - R \ln(K_{eq})}{\Delta V} \quad [2]$$

where P means pressure, T temperature, S entropy, V volume, R is the gas constant and  $K_{eq}$  the equilibrium constant. This equation describes the position of possible reaction curves within the PT field (Fig. 2.1).

Two additional equations are necessary to understand the thermodynamic constraints of geothermobarometry:

$$\Delta V_R = \Delta V_{Pr} - \Delta V_{Ed} \quad [3]$$

$$\Delta S_R = \Delta S_{Pr} - \Delta S_{Ed} \quad [4]$$

Herein, V represents volume, S entropy, R refers to reaction, Pr to products and Ed to educts. These equations describe the change of the volume and the entropy for a particular reaction. With the help of Figure 2.1 and equations [2], [3] and [4] it is possible to perform an estimation of metamorphic PT conditions.

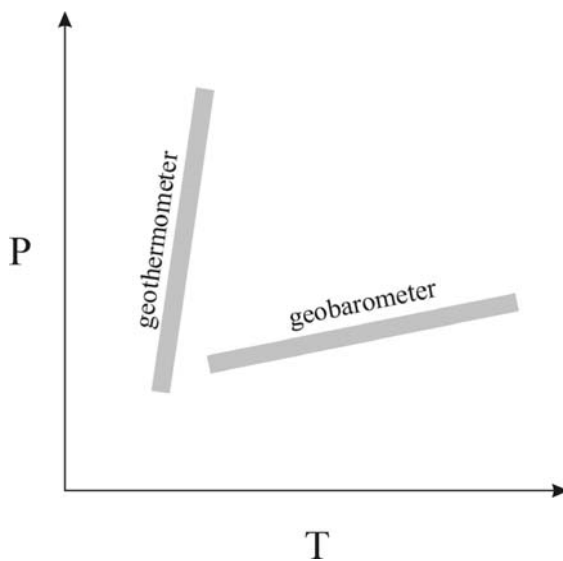


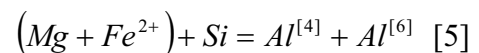
Figure 2.1: Position of reaction curves based on equation [2]. Steep slope represents a reaction useful as geothermometer, flat slope a reaction which can be used as a geobarometer.

As mentioned above, the reacting phases have to be in mineral-chemical equilibrium, which, however, is often not clear. Additionally, it is assumed that the metamorphic mineral paragenesis was formed under the highest temperature conditions the rock has ever experienced. However, these two important facts cannot be proven well and therefore they form the greatest source of error. Other effects influencing geothermobarometry are Mg and Fe exchange reactions on the retrograde PT-path, which often result in too low metamorphic temperatures. Another error may be introduced by false

estimates of the  $Fe^{2+}/Fe^{3+}$ -ratios in silicate minerals or oxides. Although charge balance constraints may provide good evidence for this ratio (e.g. in case of garnet analyses), they often fail in case of amphibole or mica analyses. Finally, there are systematic errors of the geobarometers and geothermometers due to the error of the experimental conditions or thermodynamic database. Despite all these constraints and sources of errors, geothermobarometry allows a rather precise determination of metamorphic temperature and pressure conditions.

Due to the mineralogical composition and the microstructures of the different samples observed in thin sections it is possible to assess their metamorphic grade and – in part – also temperature and pressure conditions the rocks suffered. The deformational behavior of certain minerals (calcite, quartz, feldspar; e.g. recrystallization due to bulging, subgrain rotation) and the magnitude of ductile or brittle-ductile deformation observable in the field can yield primary information about deformation temperatures.

We estimated pressure conditions of samples from both the Austroalpine nappe stack and the South Penninic mélange. We used the Si-content of phengite based on the Tschermak's substitution (equation [5]) with the graphical solution provided by Massonne and Szpurka (1997) (Fig. 2.2).



Phengite represents an intermediate member in the solid solution range between nearly ideal muscovite and Al-celadonite (e.g. Massonne and Szpurka 1997). Due to the absence of critical mineral assemblages for which this geobarometer was calibrated (K-feldspar + phlogopite + quartz, quartz + garnet + kyanite, talc + kyanite + quartz), this method only yields minimum pressure

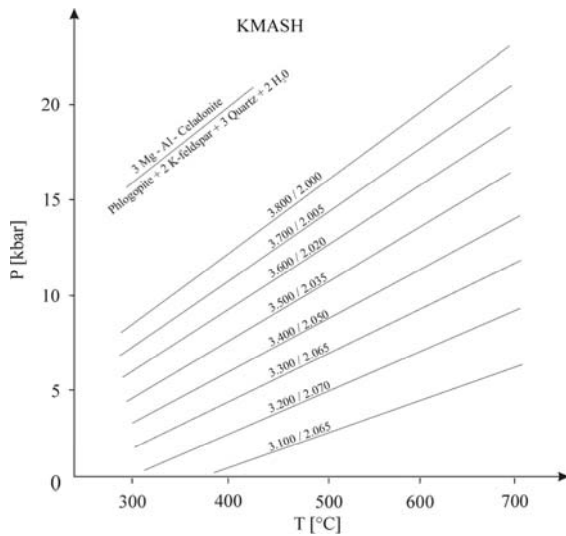


Figure 2.2: Diagram to assess the pressure conditions based on the Si content p.f.u. of phengite based on and redrawn after Massonne and Szpurka (1997). Numbers on isopleths correspond to: Si content / octahedral occupancy.

conditions. Mineral analyses were performed using a CAMECA SX100 electron microprobe operating in the wavelength-dispersive mode. Major and minor elements were determined at 15 kV acceleration voltage and a beam current of 20 nA with counting times of 20 s for major elements, and 30 s for minor elements. The beam diameter used for the mineral analyses was 5  $\mu\text{m}$  for all mineral except for plagioclase, where we used 10  $\mu\text{m}$  in order to suppress sodium diffusion. The standard sets of the Smithsonian Institute (cf. Jarosewich et al. 1980) and of MAC<sup>TM</sup> were used for reference.

#### 2.4. Image analyses

Field images and geological maps were processed with the image-processing software Scion Image (Scion Corporation). We scaled every image using a given amount of pixel per length unit. Thresholds were applied for different gray scales in order to convert the images into black and white bitmaps. Afterwards, the software automatically outlined, counted and measured the individual clasts, to analyze

their major and minor axes, and the clast area.

#### 2.5. Profile reconstruction using 2DMove

In order to relocate plate interface features to their former position we projected the investigated profiles into a composite synthetic section perpendicular to the strike of the former subduction zone. This restoration is based on the N-S section provided by Schmid et al. (1996), redrawn after the NFP-20-East seismic traverse covering the main geological and tectonical units in the working area (see Chapter 4). We used the software 2DMove (Midland Valley) for restoration. After loading the basic cross section into the software, we digitized important horizons and faults. For simplification we used only the top and the base of the South Penninic mélangé as horizons to be restored. The first restoration step was the backward movement of the vertical offset along the Engadine line using the deformation algorithm “fault parallel flow”. In a second step “line length unfolding” was applied to the folded South Penninic mélangé, which resulted in two flat lying horizons (Fig. 2.3).

#### 2.6. Provenance Analyses

Provenance analyses provide information about the origin of the source rocks and tectonic background of the metasedimentary material. Based on the ratio of stable to unstable detrital components in siliciclastic rocks (see text below) (Dickinson 1970), which was obtained by point-counting in thin sections, the provenance of the studied sediments is presented in a variety of discrimination diagrams (ternary systems, Chapter 7). Counting was performed on lithoclasts of 600 – 1000  $\mu\text{m}$  in size, in fine layers of a calcarenitic matrix.

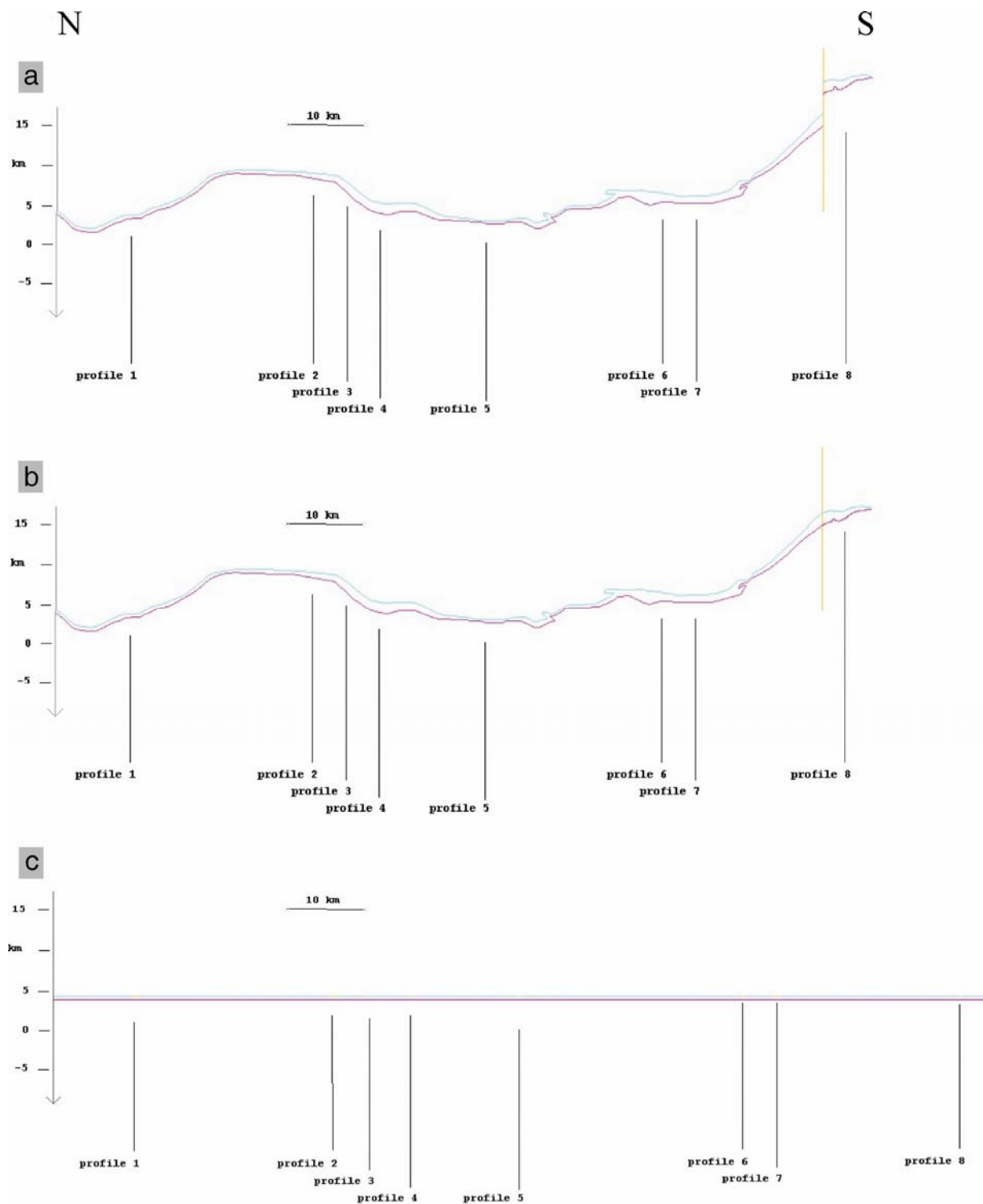


Figure 2.3: Reconstructed profiles using the Midland Valley software 2DMove. Blue line corresponds to the top of the South Penninic mélangé, red line to its base. a) digitized starting cross section, b) removal of vertical offset along the Engadine line (yellow) using "fault parallel flow", c) final result of applying the "line length unfold" algorithm to remove later deformation along the South Penninic-Austroalpine plate interface zone. This resulted in two flat lying horizons.

The components used here are defined as follows: Single quartz grains (QM) and polycrystalline quartz aggregates (QP) form the stable components, whereas single feldspar grains (F), feldspar aggregates and quartz-feldspar aggregates, also associated with mica and other minerals (QF) form part of the unstable components. These further comprise all rock fragments (L) derived from volcanic (Lv), metamorphic (Lm), and sedimentary rocks (Ls). Since for a more distinct discrimination the genetic aspect of rock provenance is of higher impact, microtextural features have always taken into account. Cherts, which are polycrystalline quartz aggregates as well, may also belong to the Ls component or represent fragments of recrystallized acid volcanic glass matrix. Similar, Lvt comprises the total number of potential magmatic rock components, i.e., QM, F, QF, and Lv. On the other hand, a QF component may also belong to Ls or Lm depending on its micro texture. As far as possible, Lv was subdivided into fragments of acid (Lva) and intermediate (? to basic) (Lvi) composition.

## 2.7. Sr isotope signatures

We studied the Rb/Sr isotope signature of marine (meta-) carbonatic samples to get information about both their age relationships and possible interaction with either crustal or mantle derived fluids. The samples are believed to have formed in a seawater environment, and thus should record the syn-precipitatorial  $^{87}\text{Sr}/^{86}\text{Sr}$  ratio of seawater, given that no later, post-depositional fluid-rock interaction occurred. The Sr-isotopic ratio of seawater is known to vary with time (e.g. Wickman 1948, Gast 1955) (Fig. 2.4), so that Sr isotopic compositions of seawater precipitates may directly be converted to absolute age information (strontium isotope stratigraphy, Look-Up Table

Version 4: 08/ 03, Howarth and McArthur 1997, McArthur et al. 2001). Several preconditions have to be met in this context, namely that no detrital components contaminated the seawater precipitates, that the Sr isotopic signature is not altered by in-situ decay of Rb, and that no secondary exchange of Sr with external fluids ever occurred. In our analytical protocol we dissolved the carbonate samples with dilute HCl and monitored Rb contents and Rb/Sr ratios of the samples. Determinations of Rb and Sr isotope ratios were carried out by thermal ionization mass spectrometry (TIMS) on a VG Sector 54 multicollector instrument (GFZ Potsdam). Sr was analyzed in dynamic mode.

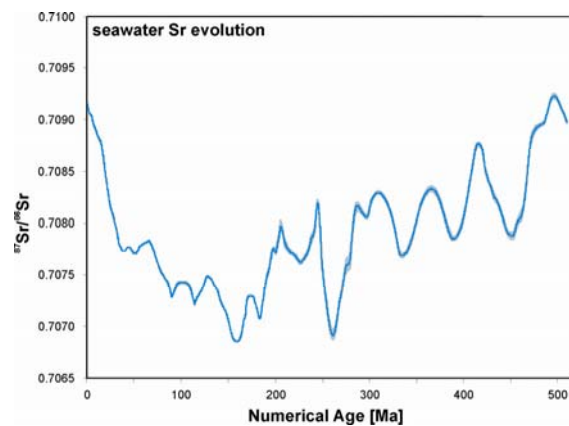


Figure 2.4: Diagram showing the Sr seawater evolution curve (McArthur et al. 2001).

## 2.8. Geochronology

### 2.8.1. Rb/Sr dating

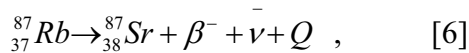
#### 2.8.1.1. The Rb/Sr isotope system

We used the Rb/Sr isotope system to shed light on the temporal constraints for the deformation along the South Penninic-Austroalpine plate interface zone. The first age determination using this method has been done by Hahn et al. in 1943. Later on, this method became into wide use due to

the accessibility of modern mass spectrometers.

Rubidium belongs to the group-1 alkali metals, and has two naturally occurring isotopes,  $^{85}\text{Rb}$  and  $^{87}\text{Rb}$ . Its ionic radius is 1.46 Å, which is quiet similar to that of potassium (1.33 Å). This allows the substitution of potassium by rubidium in all K-bearing minerals, such as mica or K-feldspar. Strontium belongs to the group-2 earth alkaline. Its ionic radius (1.13 Å) is comparable to the ionic radius of calcium (0.99 Å) allowing for the substitution of Ca by Sr in minerals like calcite, plagioclase, and apatite. Sr has four naturally occurring isotopes:  $^{88}\text{Sr}$ ,  $^{87}\text{Sr}$ ,  $^{86}\text{Sr}$  and  $^{84}\text{Sr}$ . Radiogenic  $^{87}\text{Sr}$  is formed by the decay of  $^{87}\text{Rb}$  (see text below). Due to the large geochemical difference of Rb and Sr, both elements behave rather unequal.

The Rb/Sr system is based on the decay of  $^{87}\text{Rb}$  into  $^{87}\text{Sr}$  including the irradiation of a  $\beta^-$  particle, which is expressed by the following equation:



where  $\beta^-$  represents the beta particle,  $\bar{\nu}$  an antineutrino and  $Q$  the decay energy. The decay energy  $Q$  is quiet low (0.275 MeV), which causes problems in the determination of the specific decay rate for this isotope (Faure 1986). The international used decay constant  $\lambda$  is  $1.42 \times 10^{-11} \text{ a}^{-1}$ .

The principle decay equation is expressed by:

$$D = N(e^{\lambda t} - 1), \quad [7]$$

where  $D$  represents the number of daughter nuclides,  $N$  the number of radioactive mother nuclides,  $\lambda$  is the decay constant, and  $t$  means time. For the Rb/Sr system equation [7] is modified as:

$${}^{87}\text{Sr} = {}^{87}\text{Sr}_i + {}^{87}\text{Rb}(e^{\lambda t} - 1) \quad [8]$$

Due to the fact that at  $t = 0$  the amount of  $^{87}\text{Sr}$  within the mineral has not to be 0 (because it is a naturally occurring isotope), it has to be included in equation [8] as  ${}^{87}\text{Sr}_i$ , where “i” means initial. By using mass spectrometry, not the number of atoms for one isotope is measured, but a proportion of isotopes. Therefore, one uses a stable isotope that is not produced by a decay process. For the Rb/Sr system one uses  $^{86}\text{Sr}$  due to its rather similar abundance as  $^{87}\text{Sr}$ , resulting in neither too large nor to small ratios. Therefore, the basic equation for the purpose of age determination using the Rb/Sr isotope system results in:

$$\frac{{}^{87}\text{Sr}}{{}^{86}\text{Sr}} = \left( \frac{{}^{87}\text{Sr}}{{}^{86}\text{Sr}} \right)_i + \frac{{}^{87}\text{Rb}}{{}^{86}\text{Sr}}(e^{\lambda t} - 1) \quad [9]$$

The  $^{87}\text{Sr}$  to  $^{86}\text{Sr}$  ratio can be directly measured with the mass spectrometer,  $^{87}\text{Rb}$  to  $^{86}\text{Sr}$  with the help of the isotope dilution method. The initial  $^{87}\text{Sr}$  to  $^{86}\text{Sr}$  ratio, as well as the term  $(e^{\lambda t} - 1)$  remains unknown. Therefore, one needs at least two analyses from one sample (i.e. cogenetic minerals, different physical fractions of one mineral) to solve this equation with two unknowns. Measuring several cogenetic minerals from one samples result in different data points within a x-y-diagram, where  $x$  represents the ratio of  $^{87}\text{Rb}$  to  $^{86}\text{Sr}$  and  $y$  means the ratio of  $^{87}\text{Sr}$  to  $^{86}\text{Sr}$ . With the slope of the regression line, the age of the sample can than be calculated. When all sample points fall onto the regression line, this line represent an isochron, and the diagram is called isochron diagram. Otherwise, the regression line represents an errorchron. Beside the calculation of the regression line, the MSWD value (mean standard weighted deviation) is also calculated, which expresses the quality of the data in relation to their position relative to the regression line. The result of solving

equation [9] represents a geological meaningful age only when the mineral system has remained a closed system with respect to Rb and Sr.

### 2.8.1.2. Sample preparation and analyzing procedure

The Rb/Sr isotope system of white mica is assumed to be thermally stable up to temperatures  $>500^{\circ}\text{C}$  to  $550^{\circ}\text{C}$ , but may be fully reset by dynamic recrystallization even at lower temperature (Inger and Cliff 1994, Freeman et al. 1997, Villa 1998). According to Müller et al. (1999) isotopic reequilibration between white mica and coexisting phases during mylonitization may occur at temperatures as low as  $350^{\circ}\text{C}$ . Careful correlations between microtextures and isotopic signatures, both by conventional mineral separation techniques (Müller et al. 1999, Glodny et al. submitted) and Rb/Sr microsampling (Müller et al. 2000, Cliff and Meffan-Main 2003) has shown that complete synkinematic recrystallization in mylonites is usually accompanied by isotopic reequilibration. Therefore, Rb/Sr isotopic data from penetratively deformed rocks can be used to date the different stages of mylonitic deformation, as long as deformation occurred below the temperature range for diffusional resetting. To detect possible Sr isotope inhomogeneities resulting from long-term incomplete dynamic recrystallization, from diffusional Sr redistribution, and/or from alteration processes, white mica was analysed in several, physically different (in terms of magnetic properties and/or grain size) fractions whenever possible. According to Müller et al. (1999) this approach ensures control on possible presence of unequilibrated, pre-deformational white mica relics. Care was taken to exclude material altered by weathering or late fluid-rock interaction. White mica sieve and magnetic fractions

were ground in ethanol in an agate mortar, and then sieved in ethanol to obtain pure, inclusion-free separates. All mineral concentrates were checked, and finally purified by hand-picking under a binocular microscope. Rb and Sr concentrations were determined by isotope dilution using mixed  $^{87}\text{Rb}/^{84}\text{Sr}$  spikes. Determinations of Rb and Sr isotope ratios were carried out by thermal ionization mass spectrometry (TIMS) on a VG Sector 54 multicollector instrument (GFZ Potsdam). Sr was analyzed in dynamic mode. The value obtained for  $^{87}\text{Sr}/^{86}\text{Sr}$  of NBS standard SRM 987 was  $0.710268 \pm 0.000015$  ( $n = 19$ ). The observed Rb isotopic ratios were corrected for 0.25% per a.m.u. mass fractionation. Total procedural blanks were consistently below 0.15 ng for both Rb and Sr. Because of generally low, and highly variable blank values, no blank correction was applied. Isochron parameters were calculated using the Isoplot/Ex program of Ludwig (1999). Standard errors, as derived from replicate analyses of spiked white mica samples, of  $\pm 0.005\%$  for  $^{87}\text{Sr}/^{86}\text{Sr}$ , and of  $\pm 1.5\%$  for Rb/Sr were applied in isochron age calculations.

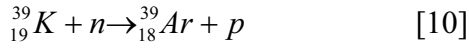
## 2.8.2. Ar/Ar dating

### 2.8.2.1. The Ar isotope system

Age dating using the Ar/Ar isotope system is a version of the K/Ar method, which was introduced by Merrihue and Turner in 1966 due to limitations in the K/Ar system caused by the very different chemical affinities of potassium and argon. Potassium is one of the major constituent of many rock-forming minerals making the K/Ar and the Ar/Ar methods widely applicable. Potassium has three naturally occurring isotopes:  $^{39}\text{K}$ ,  $^{40}\text{K}$  and  $^{41}\text{K}$ . Argon, a noble gas, has also three naturally occurring isotopes ( $^{36}\text{Ar}$ ,  $^{38}\text{Ar}$ ,  $^{40}\text{Ar}$ ).  $^{40}\text{K}$  decays to  $^{40}\text{Ca}$  and  $^{40}\text{Ar}$  via  $\beta^{-}$  decay,  $\beta^{+}$  decay and electron capture. Most

atmospheric Ar derives from this decay reaction.

More import for the use of the Ar/Ar method is the decay of  $^{39}\text{K}$  into  $^{39}\text{Ar}$ , which is forced in a nuclear reactor by irradiation with fast neutrons:



Within this equation  $n$  represents neutron capture and  $p$  proton emission. The potassium content of a sample is constrained by its amount of argon. Otherwise,  $^{39}\text{Ar}$  is a radioactive element, which decays back into  $^{39}\text{K}$  with a half life time of 269 a. Due to this half life time the amount of  $^{39}\text{Ar}$  is assumed as constant over the time of Ar/Ar analyses.

The production of  $^{39}\text{Ar}$  from  $^{39}\text{K}$  during irradiation is expressed by:

$$^{39}\text{Ar} = ^{39}\text{K} \Delta t \int_{\min e}^{\max e} \varphi_e \sigma_e de \quad [11]$$

where  $t$  means time,  $\varphi_e$  stands for the flux density of neutrons with energy  $e$ , and  $\sigma_e$  is the capture cross section of  $^{39}\text{K}$  for neutrons of energy  $e$ .

The principle decay equation [7] adjusted for this method results in:

$$^{40}\text{Ar}_{\text{total}} = ^{40}\text{Ar}_i + \frac{\lambda_{\text{EC}}}{\lambda_{\text{total}}} ^{40}\text{K} (e^{\lambda_{\text{total}} t} - 1) \quad [12]$$

where  $^{40}\text{Ar}_i$  means the initial amount of  $^{40}\text{Ar}$  at  $t = 0$ , and  $\lambda_{\text{EC}}$  stands for the electron capture decay constant.

Combining equation [11] with equation [12] results in:

$$\frac{^{40}\text{Ar}^*}{^{39}\text{Ar}} = \left( \frac{\lambda_{\text{EC}}}{\lambda_{\text{total}}} \frac{^{40}\text{K}}{^{39}\text{K} \Delta t \int \varphi_e \sigma_e de} \right) (e^{\lambda_{\text{total}} t} - 1) \quad [13]$$

where  $^{40}\text{Ar}^*$  represents the radiogenic argon.

During the course of irradiation within the reactor, a standard of known age is irradiated in addition to the sample. The term in large parentheses in equation [13] remains the same for both the sample and the standard, and is used as a single quantity. Its reciprocal is called  $J$  is evaluated as a constant (Mitchell 1968). The age is calculated by rearranging equation [13] into:

$$t = \frac{1}{\lambda} \ln \left[ J \left( \frac{^{40}\text{Ar}^*}{^{39}\text{Ar}} \right) + 1 \right] \quad [14]$$

In addition, irradiation corrections have to be applied, because Ar isotopes are also generated from calcium and other potassium isotopes than  $^{39}\text{K}$  by neutron reactions.

For Ar/Ar geochronology the method of stepwise heating is widely used. Argon is expelled from the sample in different temperature steps, and simultaneously measured in a mass spectrometer. Ar isotopes are calculated for each step, being the same for all steps in an ideal case. Due to excess argon (captured Ar from other sources) or argon loss (less bonded Ar in the outer rims of analyzed grains) this is often not the case. In these circumstances, the analysed sample is expected to reach a plateau, after rise and fall of the calculated ages. This plateau is assumed to represent a geological meaningful age. For our purpose of Ar/Ar geochronology on pseudotachylytes we used the method of laser ablation as recommended by Müller et al. (2002) (see text below).



### 2.8.2.2. *Sample preparation and analyzing procedure*

We used the Ar/Ar method to date brittle deformation and associated formation of pseudotachylytes. In an initial phase, we macroscopically selected pseudotachylytes, which appear to be undeformed and less altered. Petrographic microscopy was used to study the chosen samples in more detail in terms of amount and petrography of clasts embedded within the fine grained pseudotachylyte matrix. Afterwards, 300  $\mu\text{m}$  thick slices of pseudotachylytes were produced and highly polished on both sides. Then, these slices were cut into small pieces of roughly 5 x 5 mm, and were checked using a binocular microscope to avoid embedded clasts, which would represent an error source for excess argon. Care was taken to exclude material altered by weathering or fluid-rock interaction. Samples were washed in de-ionized water to remove fine powder on the surface of grains (health risk after irradiation). After washing, grains were dried in an oven at roughly 100°C.

For irradiation, samples were individually wrapped in Al foil and then packed into holes within a 99.999 % pure Al disk. Samples were irradiated for four days in a reactor at the GKSS Geesthacht. After the irradiated samples returned from the reactor, the Al foils were opened and the samples were recollected for subsequent argon isotope analyses. The grains were loaded into holes within a Cu disk. This disk was finally introduced into a vacuum line at the Ar laboratory of the University of Potsdam. We used an automated laser extraction and gas cleanup system operating with both a Merchantek LUV266X quadrupled laser emitting UV at 266 nm and a Merchantek floating MIR10IR (CO<sub>2</sub>) (20W Nd-YAG) laser. These laser systems allow both in-situ ablation of small spots on the samples and bulk step-heating. After extraction of Ar

gas from the sample by step heating (several steps until total fusion), the gas was purified in the ultra high vacuum analytical line. Ar gas was introduced into a Micromass 5400 Static Vacuum Mass Spectrometer. Then, the isotopic ratios were obtained. Finally, obtained data were used to produce isochron and plateau plots, and ages were calculated using the Isoplot/Ex program of Ludwig (1999). Analytical errors were applied within the calculation using weighted errors. The validity of isochron plots was checked with the MSWD values (see Chapter 2.8.1.1.). Data of the different analyses are summarized in the appendix.

